

Chemical functionalization, electronic and dielectric properties of hybrid organic-tin layers

Andre Oliveira

*Universidade Federal de Goiás, Institute of Physics,
Campus Samambaia, 74690-900 Goiânia, Goiás, Brazil*

Andreia Luisa da Rosa

*Universidade Federal de Goiás, Institute of Physics,
Campus Samambaia, 74690-900 Goiânia, Goiás, Brazil and
Bremen Center for Computational Materials Science,
University of Bremen, Am Fallturm 1, 28359 Bremen, Germany*

Thomas Frauenheim

*Bremen Center for Computational Materials Science,
University of Bremen, Am Fallturm 1, 28359 Bremen, Germany and
Computational Science Research Center, No.10 East Xibeiwang Road,
Beijing 100193 and Computational Science and Applied Research Institute Shenzhen, China.*

Abstract

Band gap tuning and dielectric properties of small organic ligands adsorbed on tin monolayers (stanene) have been investigated using first-principles calculations. Charge density analysis using density-functional theory shows that the ligands are chemisorbed on stanene and some of the groups can open a band gap in the originally metallic stanene. Furthermore many-body GW calculations demonstrate that the dielectric properties of bare and ligand adsorbed stanene have a large anisotropy. Our findings of a finite gap opens a path for rational theoretical design of functionalized two-dimensional stanene.

I. INTRODUCTION

Graphene in its honeycomb structure has a zero gap, with conduction and valence bands being degenerate at K and K' points, forming Dirac cones with charge carriers which are massless fermions^{1,2}. Graphene has a metallic behavior and opening a band gap in graphene has been challenging. In general, for the creation of optical and electronic devices semiconductor properties are desirable. Two-dimensional nanostructures built from group 14 elements, such as tin, silicon and germanium have been the topic of several investigations³. In fact, stanene has already been demonstrated on substrates such as Bi₂Te₃⁴ and Ag(111)⁵. From the theoretical side, first-principles molecular dynamics have shown that bare stanene has a phonon dispersion without imaginary frequencies and the monolayer is thermally stable up to 700 K⁶.

Similarly to graphene, stanene has a metallic behavior. Some ways of opening a band gap in stanene include doping by impurities, defect engineering, functionalization with organic and/or biological molecules^{7,8} and applied electric field and applied strain⁹. A promising route for surface functionalization of two-dimensional materials was demonstrated using adsorption of organic molecules or functional groups, as it has been reported for germanene¹⁰. However, experimental results on functionalized stanene are still missing.

In this work we have investigated the electronic and dielectric properties of stanene with small organic groups using first-principles calculations. We show that some of the adsorbed stanene are suitable for opening a band gap in the metallic stanene. We also show that the dielectric properties of this material have a large anisotropy, with absorption in the visible region, which could render possible applications in optoelectronic devices.

II. METHODOLOGY

We employ density functional theory^{11,12} within the generalized gradient approximation¹³ and the projected augmented wave method (PAW)^{14,15} as implemented in the VASP code¹⁵ to investigate the electronic structure of hybrid stanene monolayers. (1×1) and (2×2) supercells were employed to simulate full and partial ligand coverages. Forces on atoms were converged until 10⁻⁴ eV/Å. A vacuum region of 10 Å is sufficient to avoid spurious interactions between stanene layers in neighbouring cells. A (8×8×1) **k**-point sampling has

been used in the calculations of all investigated systems with an energy cutoff of 400 eV. The calculation of the dielectric function was performed using the GW method¹⁶ with a $(6 \times 6 \times 1)$ \mathbf{k} -points mesh.

III. RESULTS AND DISCUSSIONS

A. Structural properties

The structural stability of the buckled and planar structure has been investigated by varying the in-plane lattice parameter a and fully relaxing all the atoms in the unit cell. The relaxed energetically most stable bare buckled structure is shown in Fig. 2(a) (side view) and Fig. 2(c) (top view). The optimized in-plane lattice parameter for buckled (planar) stanene is $a = 4.67 \text{ \AA}$ (4.85 \AA). The buckled structure is 0.31 eV energetically more stable than the planar one. The Sn-Sn distance is 3.01 \AA , as shown in Table I. The calculated band structure of buckled stanene is shown in Fig. 1 (b) and density-of-states (DOS) as shown in Fig. 1 (d). Stanene has a metallic character with small gap.

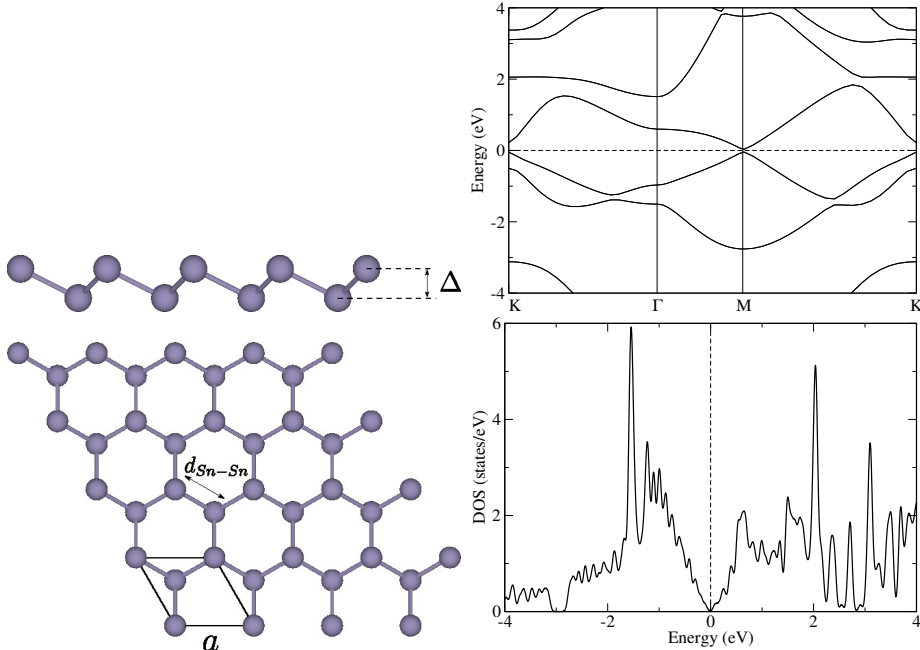


FIG. 1: a) top view, b) side view, c) density of states and d) band structure of optimized tin layers within GGA.

Calculations for the following ligands -H, -OH, -CH₃, -C₂H, -I and -F have been performed.

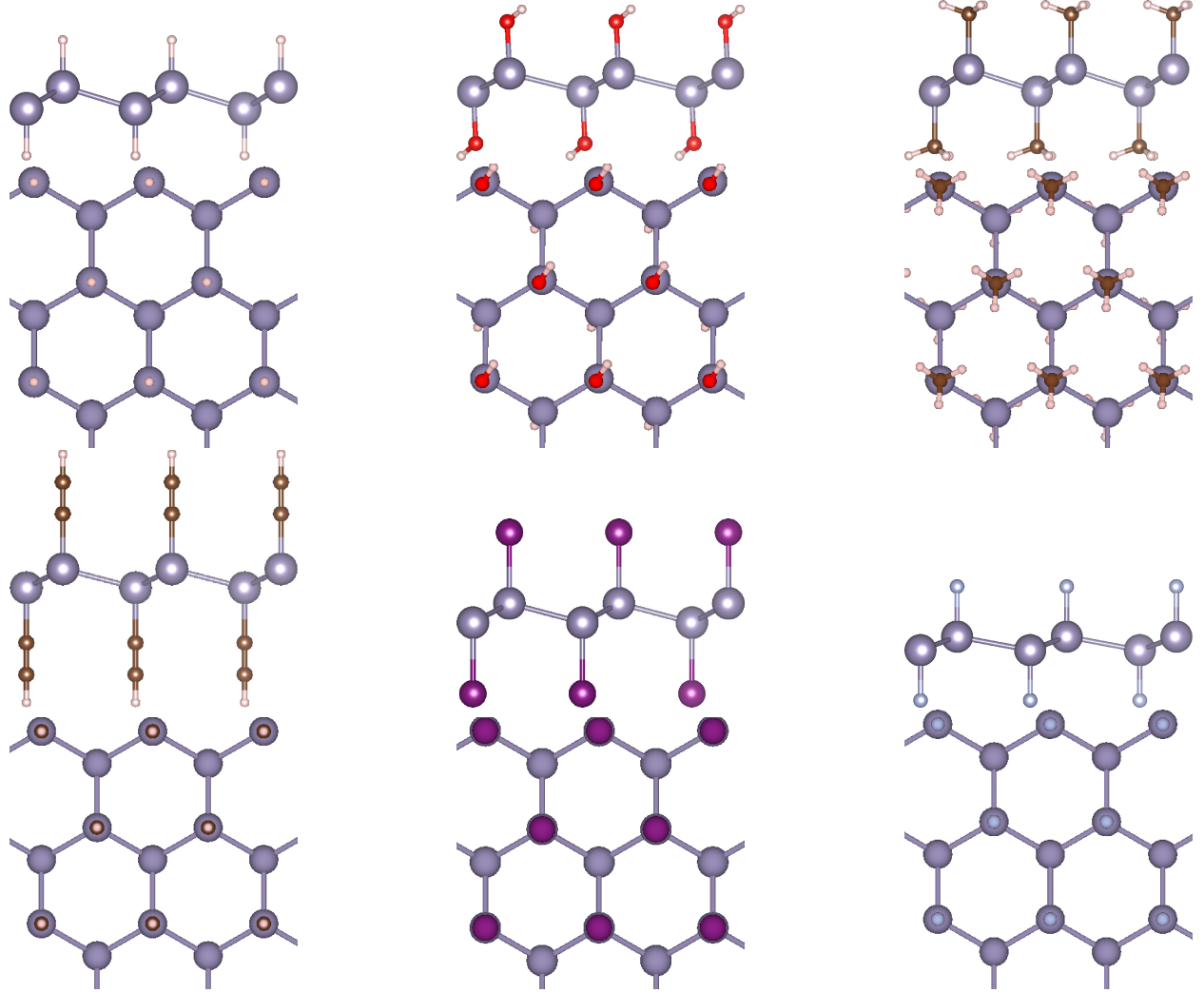


FIG. 2: Side view of relaxed tin layers adsorbed with organic ligands at one monolayer regime: a) -H, b) -OH, c) -CH₃, d) C₂H, e) -I and f) -F. Red, brown, blue, white and magenta are oxygen, carbon, hydrogen and germanium atoms, respectively.

We have analyzed their relaxation, charge density distribution, band structure and dielectric function. The relaxed structures of functionalized stanene are shown in Fig. 2.

Upon adsorption of ligands, the initially buckled geometry of stanene has a slight different buckling compared to the bare stanene, as shown in Table I. Hybrid stanene structures have a similar behavior to hybrid germanene where a small buckling is reported^{17–20}. This is rather different from what has been found for similar organic ligands on group-V nanostructures which become planar upon adsorption^{21,22}. As a general feature, the intralayer lattice parameter a and consequently Sn-Sn distance are slightly dependent on the ligand type. On the other hand, the ligand-stanene interaction should play an important role on the

ligand	$a(\text{\AA})$	$d_{Sn-Sn}(\text{\AA})$	$d_X(\text{\AA})$	$\Delta(\text{\AA})$	$E_{gap}(\text{eV})$
					PBE
-H	4.71	2.86	1.74	0.79	0.26
-OH	4.89	2.88	2.02	0.66	0.22
-CH ₃	4.73	2.88	2.21	0.86	0.16
-C ₂ H	4.84	2.92	2.12	0.67	0.22
-I	4.90	2.83	2.73	0.86	0.34
-F	4.99	2.93	1.96	0.53	0.28

TABLE I: Lattice parameter a , in-plane Sn-Sn distance d_{Sn-Sn} , Sn-X distance d_{Sn-X} , buckling Δ , band gap E_{gap} and formation energy E_f of functionalized stanene.

stabilization of the hybrid structures.

In Fig. 2 (a) is the Sn-H distance is 1.74 Å with Sn-Sn bond length d of 2.86(Å). The Sn-OH structure is shown in Fig. 2 (b) and has $a = 2.02$ Å and Sn-Sn distance $d = 2.88$ Å. The Sn – CH₃ structure shown in Fig. 2 (c) has $a = 2.21$ Å and Sn-Sn distance d of 2.88 Å. The in-plane lattice constant is slightly lower for Sn – C₂H shown in Fig. 2 (d) (2.12 Å). In Fig. 2 (e) the functionalization with I is seen. It has a Sn-I distance of 2.73 Å and Sn-Sn bond lengths of 2.83 Å. Finally for Sn-F one has Sn-F equal to 1.96 Å and Sn-Sn of 2.93 Å. As the ligands we consider here are small, ligand-Sn interaction should play a major role in stabilizing hybrid Sn-ligand structures.

IV. CHARGE DENSITY DIFFERENCE

The nature of the chemical bonds in the hybrid systems was investigated by calculating the charge density difference between the electronic densities of the adsorbed stanene and their constituent systems. The electronic density difference shown in Fig. 3 is given by $\Delta\rho = \rho^{Sn-X} - \rho^{Sn} - \rho^{-X}$, where ρ^{Sn-X} is the electronic density of the hybrid Sn-X layers, ρ^{Sn} and ρ^{-X} are the charge densities of stanene and the ligand, respectively, calculated at fixed atomic positions after structure optimization of the hybrid layers. As a general feature, charge accumulation on the ligand (yellow) and charge withdrawal (blue) close to the tin atom is seen.

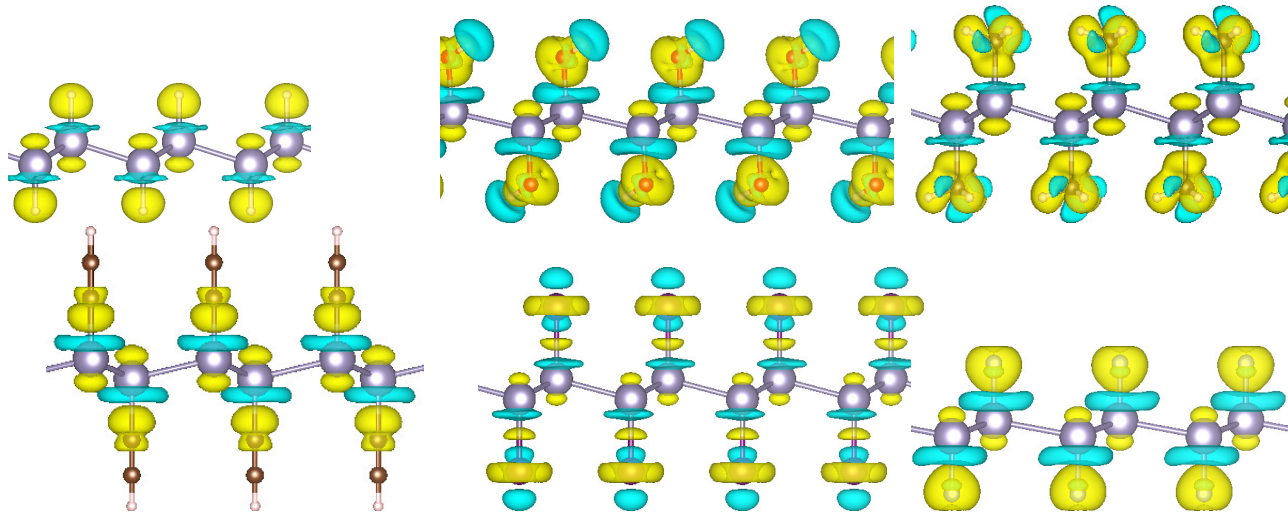


FIG. 3: Charge density difference of modified stanene structures with a) -H, b) -OH, c) -CH₃, d) C₂H, e) -I and f) -F. Blue indicates a loss of electrons whereas yellow indicates accumulation of electrons. Isosurface levels are set to $0.002 e/\text{\AA}^3$.

Sn-H hybrid layers shown in Fig. 3(a) have a larger electron density at hydrogen atoms and a withdraw of electrons at tin sites. Sn-OH also shows accumulation of charge at the ligand, mainly on oxygen and carbon atoms, while charge is withdrawn at tin sites as shown in Fig. 3(b). The complex Sn-CH₃ shows that electronic charge is accumulated the ligand upon adsorption on stanene. Furthermore, between C and Sn bonds there is an excess of electrons as it can be seen in Fig. 3(c). The Sn-C₂H hybrid also shows accumulation of charge at the ligand, mainly on the oxygen and carbon atoms, while charge is depleted at the tin site, as shown in Fig. 3(d). The complex Sn-I also shows accumulation of electrons on the ligand oxygen and carbon atoms, while regions close to the tin are depleted of electrons. At the tin site and also between C and Sn bonds there is an excess of electrons as seen in Fig. 3(e). The complex Sn-F also shows accumulation of electrons on the ligand oxygen and carbon atoms, while regions close to the tin are depleted of electrons. At the tin site and also between C and Sn bonds there is an excess of electrons as seen in Fig. 3(f).

One can therefore conclude that due to the charge accumulation/withdraw in the modified tin layers, the reactivity of the whole system changes. This feature could be quite useful for further functionalization of organic or biomolecules. Taking into the account the electronegativity trend in the periodic table, we have the following order for electronegativity: $F > I$ and $C \approx I$, as calculated in Ref.²³. These calculations allowed determine the correla-

tion between the electronegativity between Sn and CH₃ and H groups. According to these calculations, it is expected that the electron affinity follows: Sn-F > Sn-H > Sn-CH₃. If we consider our results for the adsorbed stanene, our results corroborate with these trends.

A. Electronic properties

In order to understand the interaction between ligand and the substrate, we have calculated the band structure, as shown in Fig. 4(a)-(f). The projected DOS is shown in Fig. 5. Bare stanene have a metallic character and zero gap with a linear dispersion at the Γ point, as it is seen in Fig. 4 (a). All organic groups can open a gap in stanene. Our results are in agreement with the ones reported in Refs. ^{3,7,8}. Energy gaps are reported in Table I.

The band structure for Sn-H is shown in Fig. 4(a) for Sn-H, Fig. 4(b) for -OH, Fig. 4(c) for Sn - CH₃, Fig. 4(d), Sn-C₂H, Fig. 4(e) for -I and Fig. 4(f) for -F.

Contributions to the states close to the Dirac point are mainly due to Sn-*p* orbitals. Upon ligand adsorption on stanene, Rashba splitting is more emphasized for -OH, I and F groups. I and F are more electronegative and therefore induces band gap opening. This means that the ligand character is also important to determine the bond strength and consequently the electronic structure of the hybrid system. We can clearly see contributions from the functional groups at VBM and CBM, implying that we have formation of bonds between the ligand and tin.

In order to verify the influence of ligand coverage on the stanene band structure, we have further investigated adsorption at different ligand-ligand separations. We employ a (2×2) unit cell with three different geometries. As a representative system we consider the Sn-C₂H structure. In Fig. 6 we show the top views of hybrid Sn-C₂H layers with partial coverage. In Fig. 6 (a) we show a (2×2) supercell at 1/8 ML coverage regime with a single molecule, in Fig. 6 (b) at 1/4 ML regime with two molecules on the opposite sides of stanene, Fig. 6 (c) at 1/4 ML coverage regime with two molecules on the same side. All these structures should be representative of possible realisable experiments. As a matter of comparison, structures with molecules adsorbed on one side should represent functionalization of stanene grown on a substrate for example ⁴ whereas structures with molecules adsorbed on both sides can be achieved by deintercalation, a method proposed for germanium layers ²⁴.

The corresponding electronic projected DOS are shown in Figs. 6(a)-(c). All systems have

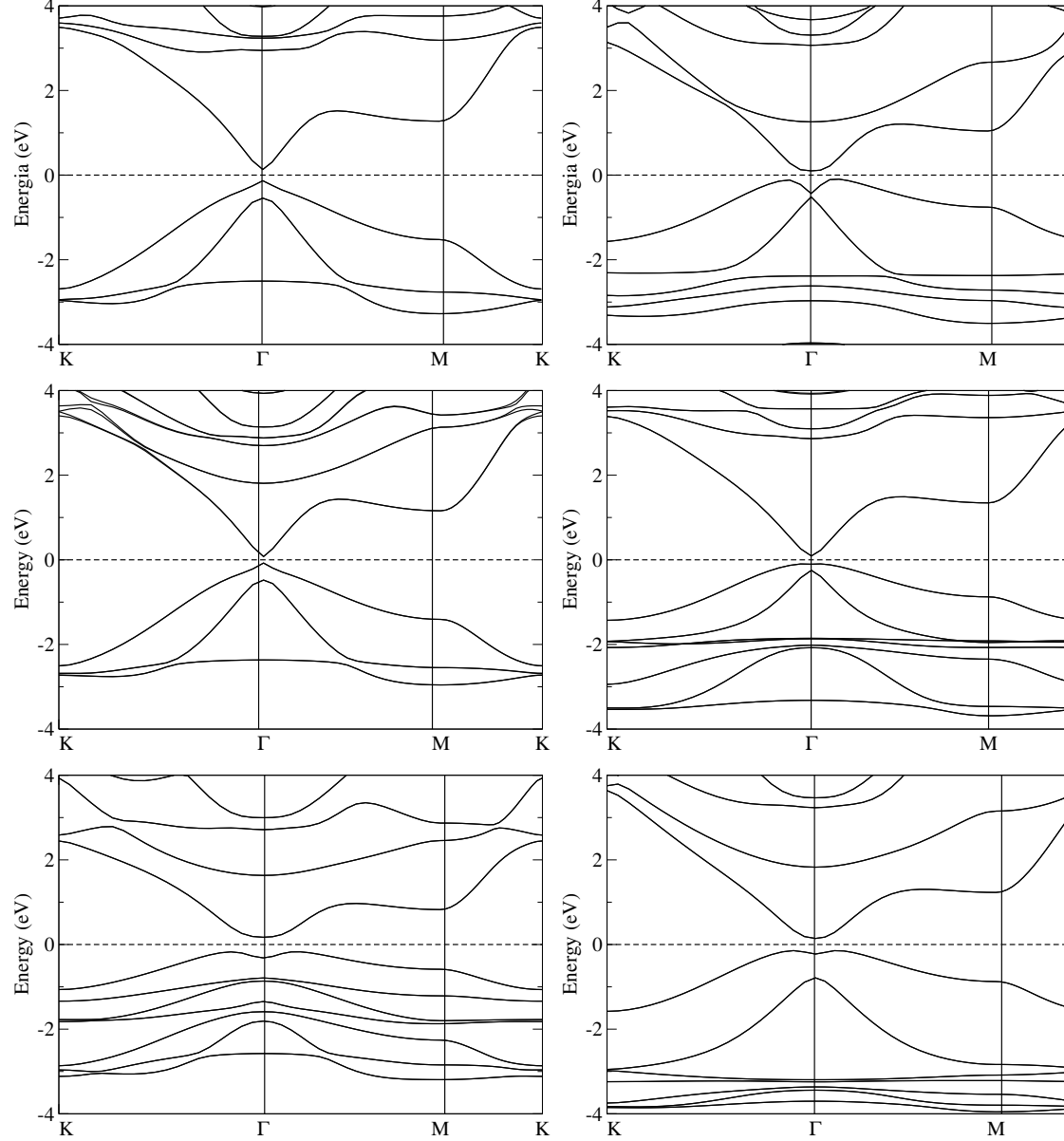


FIG. 4: Band structure of modified stanene structures. a) -H, b) -OH, c) -CH₃, d) -C₂H, e) -I and f) F. The zero of energy is set at zero.

a metallic behavior. This means that not all configurations and coverages would lead to band gap opening. It would be necessary to have ligands more densely packed to open a small, but still sizeable band gap in stanene. We can therefore conclude that the ligand-ligand interaction does play a role in the band gap opening of stanene.

The dielectric function of hybrid stanene-organics layers were investigated by calculating the imaginary part of the dielectric function at GW level. The imaginary part of the dielectric

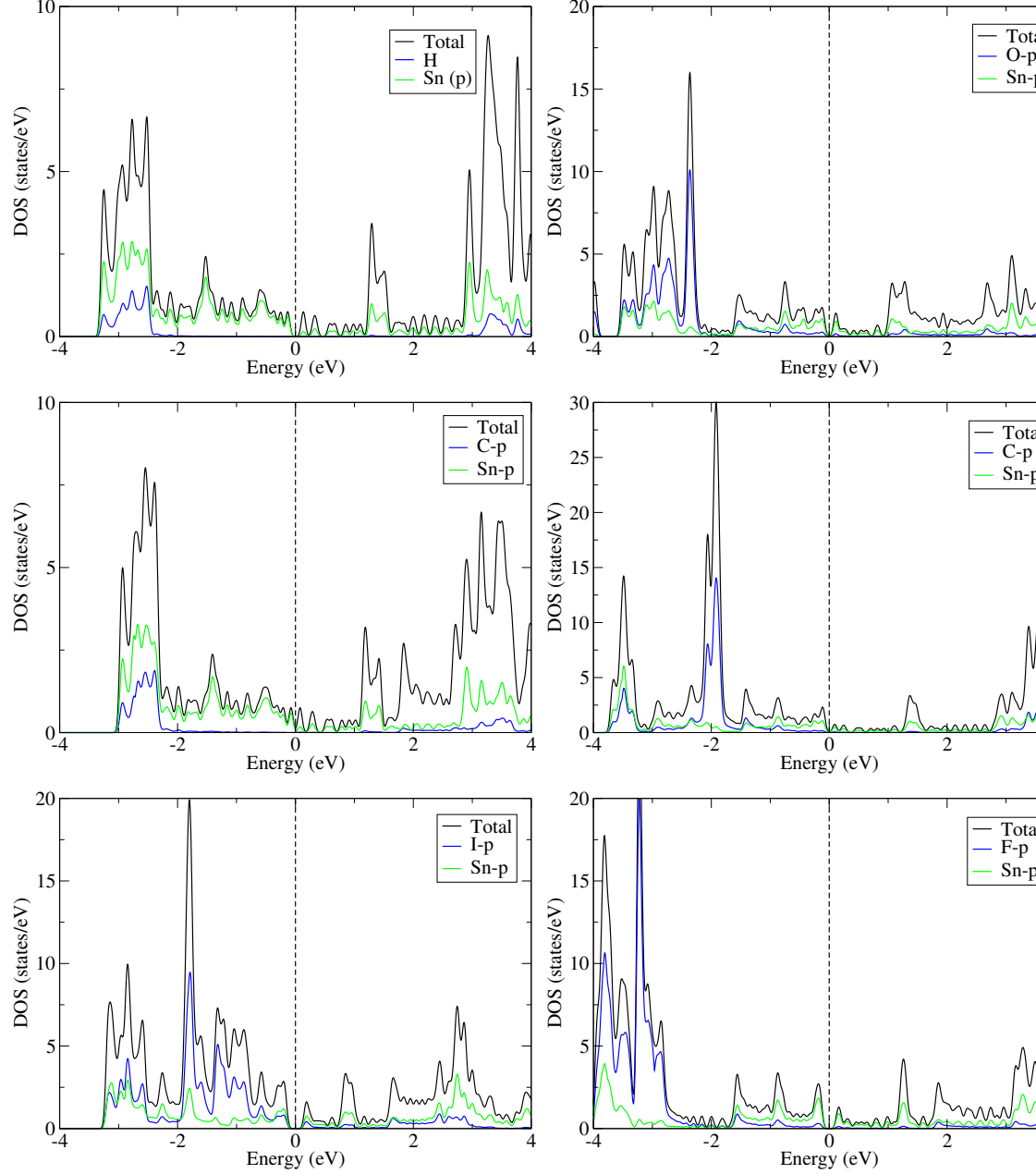


FIG. 5: Atom projected density of states DOS of modified stanene structures. a) -H, b) -OH, c) -CH₃, d) -C₂H, e) -I and f) F. The zero of energy is set at zero.

function is calculated directly from the electronic structure through the joint density of states and the momentum matrix elements occupied and unoccupied eigenstates according Ref. ¹⁶.

The bang gaps obtained within GGA, HSE and GW₀@HSE are reported in Table II. One noticed that there is an improvement for H, CH₃, C₂H for HSE compared to GGA. GW compared to HSE there is an improvement for H, CH₃, C₂H and a bit for I and F and none

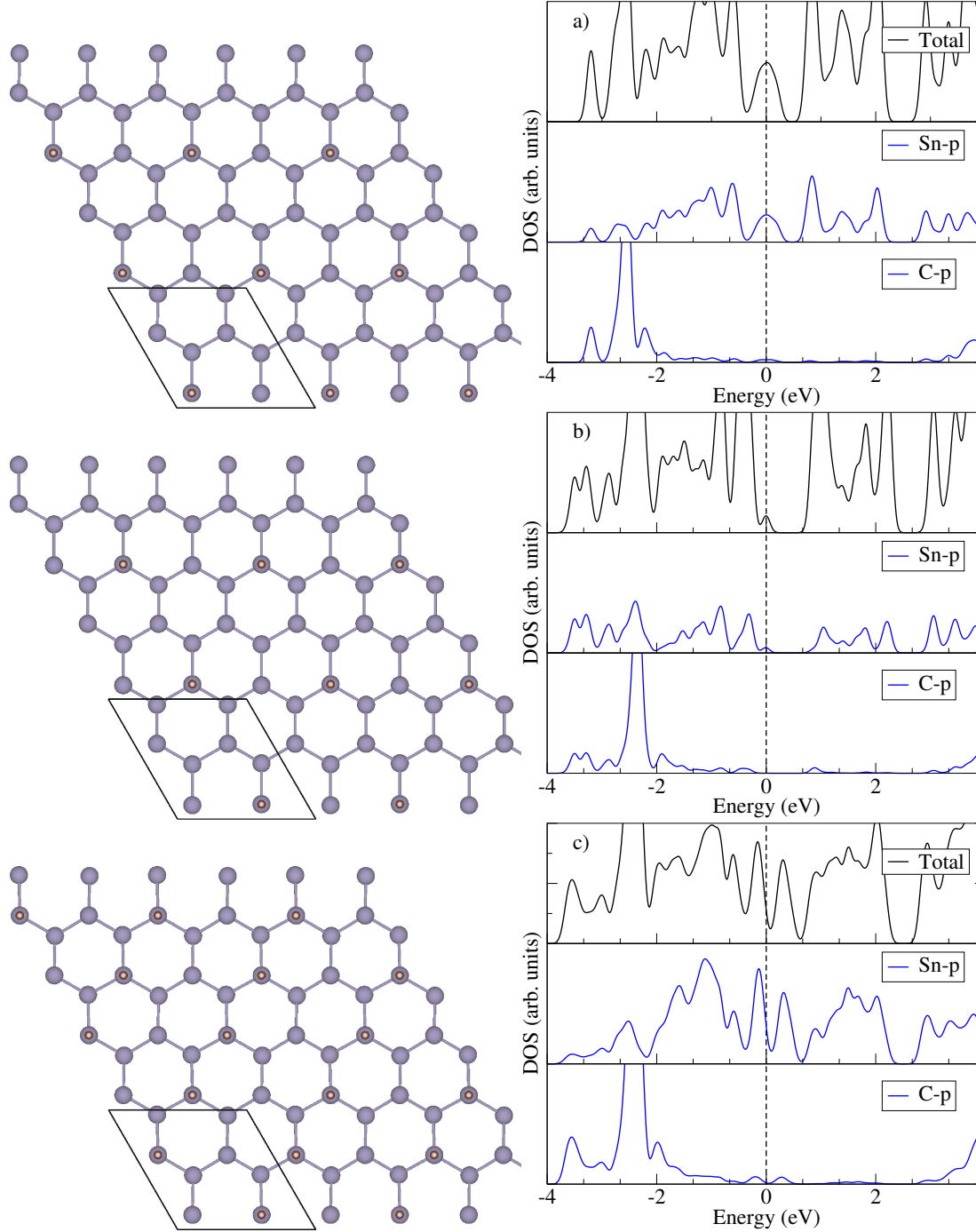


FIG. 6: Top views Orbital projected DOS of hybrid Sn-C₂H layers at: a) 1/8 ML regime with one molecule, b) 1/4 ML regime with two molecules on opposite sides, c) 1/4 ML regime with two molecules on the same side. Brown, blue and white spheres are carbon, hydrogen and tin atoms, respectively. Fermi level is set at zero.

for OH.

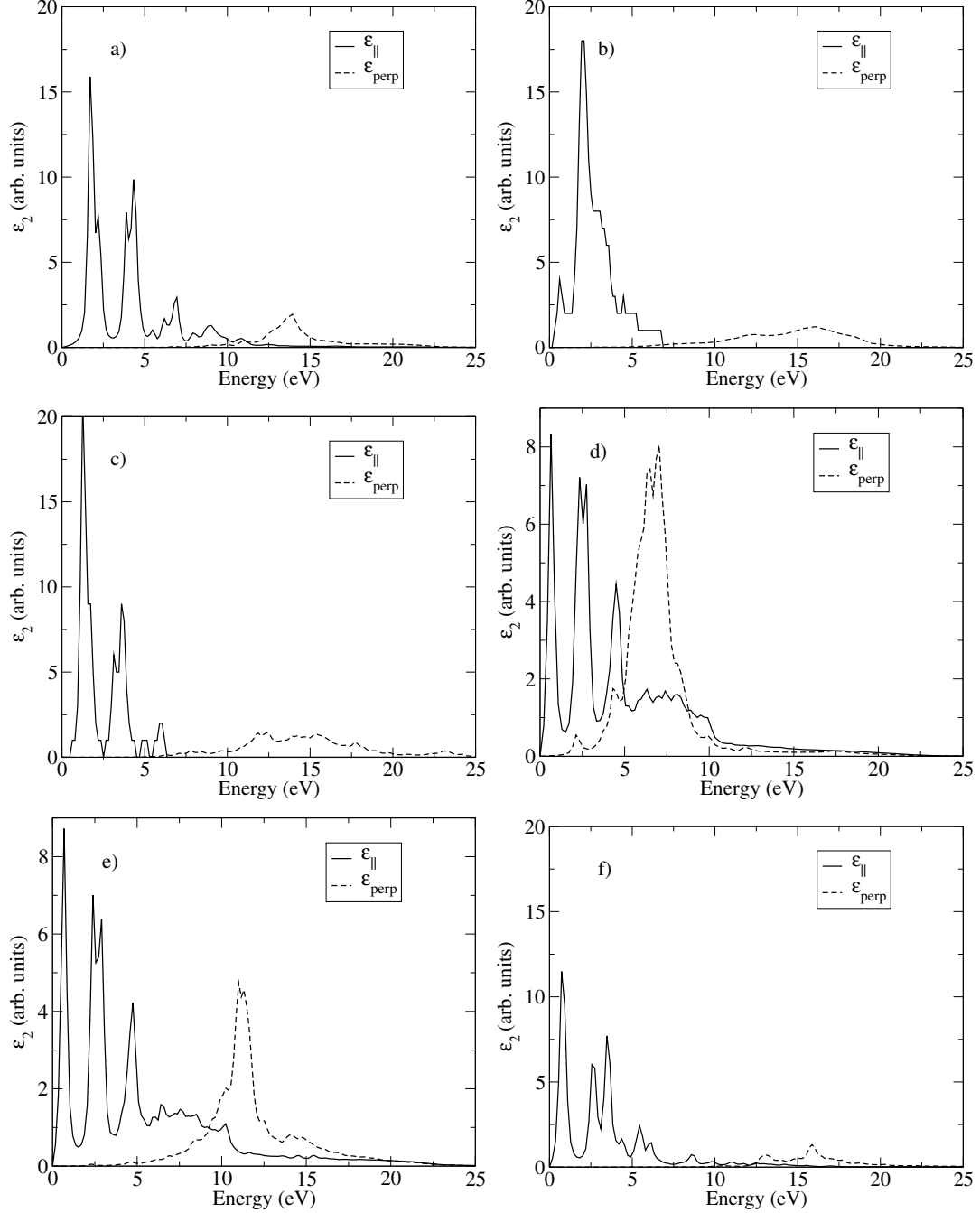


FIG. 7: Imaginary part of the dielectric function for pure and functionalized stanene within GW_0 approximations. a) H, b) -OH, c) - CH_3 , d) - C_2H , e) -I and f) -F. Light propagation parallel and perpendicular to the tin layer is denoted as $\epsilon_{\parallel} = (\epsilon_{xx} + \epsilon_{yy})/2$ and $\epsilon_{\text{perp}} = \epsilon_{zz}$, respectively.

We show the dielectric function calculated within the G_0W_0 and GW approximations in Fig. 7. The averaged parallel $\varepsilon_{\parallel} = (\varepsilon_{xx} + \varepsilon_{yy})/2$ and perpendicular $\varepsilon_{\perp} = \varepsilon_{zz}$ components of the imaginary part of the dielectric function ε_2 are shown. The ε_{\parallel} component corresponds to the propagation of the external electromagnetic field parallel to the stanene plane while ε_{\perp} corresponds to the field perpendicular to the plane. Because of optical selection rules, anisotropy in the optical spectra is seen. Anisotropy has also been reported in layered monochalcogenide of tin sulfide (GeS)²⁵, black phosphorous²⁶ and bismuthene^{21,27}. The systems with a gap show finite absorption limits for both parallel and perpendicular directions with larger intensity for the (ε_{\parallel} component).

As discussed in Ref.²⁴, both ligand size and electronegativity can change the bond length and band gap of functionalized germanene. Larger ligands are expected to lead to larger Sn-Sn separation, thus yielding a lower band gap. Ligands with greater electronegativity are expected to withdraw electrons and therefore lower the band gap. The general conclusion is that ligands that are more electron-withdrawing and have greater steric bulk will expand the Sn-Sn framework and lower the band gap, with complete ligand coverage.

The bare stanene shown in Fig. 7(a) has metallic behavior.

Except for -OH, I and -F groups, HSE does not lead to improvement in the band gap. Interestingly enough, water does not dissociate on stanene²⁸. The water adsorption is stable on stanene, as reported in Ref.²⁹, which could explain the low formation energy of -OH groups. On the other hand, -OH groups are still able to modify the band structure of stanene by opening a large gap of 0.22 eV. Besides, -OH groups were found to lead to Quantum Spin Hall (QSH) effects in stanene³⁰, making them promising for optoelectronic devices. GW calculations were found to lead to further improvement compare to HSE for H, CH₃, C₂H, I and F. Larger improvement for covalent type bonds such as for H, CH₃ and C₂H.

As a general feature, two main absorption peaks appear in the spectrum for all groups, except for -OH. Sn-H shown in Fig. 7(a) has peaks at 1.64 and 4.21 eV. The Sn-OH spectrum shown in Fig. 7(b) has peak at 2.05 eV. A first peak at 1.42 for Sn-CH₃ is seen in Fig. 7(c). A second peak appears at 3.48 eV. For -C₂H one has peaks at 0.75 and 2.50 eV as it can be seen in Fig. 7(d). -I and -F have peaks at similar positions, as seen in Figs. 7(e) and (f). This could be due the similar electronegativity

ligand	$E_{gap}(\text{eV})$		1st peak	2nd peak
	HSE	GW ₀		
-H	0.50	1.10	1.64	4.21
-OH	0.19	0.18	2.05	-
-CH ₃	0.37	1.05	1.42	3.48
-C ₂ H	0.38	0.62	0.75	2.50
-I	0.34	0.60	0.70	2.60
-F	0.30	0.62	0.75	2.61

TABLE II: Gw₀ band gap E_{gap} and first and second energy transitions of functionalized stanene.

V. CONCLUSIONS

We have performed first-principles calculations of stanene functionalized layers with small organic groups. Our charge density analysis show that the ligands are chemisorbed on the tin layers. Our calculations for the dielectric properties of bare and ligand adsorbed stanene show a large anisotropy and that the absorption onset is determined by ligand electronegativity. We believe our findings of a finite gap shows open a path for rational design of nanostructures with possible applications in biosensors and solar cells.

VI. ACKNOWLEDGEMENTS

We acknowledge the financial support from the Brazilian Agency CNPq and German Science Foundation (DFG) under the program FOR1616. The calculations have been performed using the computational facilities of Supercomputer Santos Dumont and at QM3 cluster at the Bremen Center for Computational Materials Science and CENAPAD.

¹ K. Novoselov, A. Geim, S. Morozov, D. Jiang, Y. Zhang, S. Dubonos, I. Grigorieva, and A. Firsov, *Science* **306**, 666 (2004).

² A. K. Geim and K. S. Novoselov, *Nature Materials* **6**, 183 (2007).

- ³ P. Tang, P. Chen, W. Cao, H. Huang, S. Cahangirov, L. Xian, Y. Xu, S.-C. Zhang, W. Duan, and A. Rubio, *Physical Review B* **90**, 121408 (2014).
- ⁴ Z. Ni, E. Minamitani, Y. Ando, and S. Watanabe, *Physical Review B* **96**, 075427 (2017).
- ⁵ M. Maniraj, B. Stadtmüller, D. Jungkenn, M. Dvel, S. Emmerich, W. Shi, J. Stöckl, L. Lyu, J. Kollamana, Z. Wei, et al., *Commun. Phys.* **2**, 12 (2019).
- ⁶ B. Peng, H. Zhang, H. Shao, Y. Xu, X. Zhang, and H. Zhu, *Scientific reports* **6**, 20225 (2016).
- ⁷ R.-W. Zhang, C.-W. Zhang, W.-X. Ji, S.-S. Li, S.-J. Hu, S.-S. Yan, P. Li, P.-J. Wang, and F. Li, *New Journal of Physics* **17**, 083036 (2015).
- ⁸ R.-W. Zhang, C.-W. Zhang, W.-X. Ji, S.-S. Li, S.-S. Yan, S.-J. Hu, P. Li, P.-J. Wang, and F. Li, *Sci. Rep.* **6**, 8879 (2016).
- ⁹ B. van den Broek, M. Houssa, E. Scalise, G. Pourtois, V. V. Afanasev, and A. Stesmans, *2D Materials* **1**, 021004 (2014).
- ¹⁰ Y. Ren and Z. Q. and Qian Niu, *Reports on Progress in Physics* **79**, 066501 (2016).
- ¹¹ P. Hohenberg and W. Kohn, *Phys. Rev.* **136**, B864 (1964), URL <http://link.aps.org/doi/10.1103/PhysRev.136.B864>.
- ¹² W. Kohn and L. J. Sham, *Phys. Rev.* **140**, A1133 (1965), URL <http://link.aps.org/doi/10.1103/PhysRev.140.A1133>.
- ¹³ J. P. Perdew, K. Burke, and M. Ernzerhof, *Phys. Rev. Lett.* **77**, 3865 (1996), URL <http://link.aps.org/doi/10.1103/PhysRevLett.77.3865>.
- ¹⁴ P. E. Blöchl, *Phys. Rev. B* **50**, 17953 (1994), URL <http://link.aps.org/doi/10.1103/PhysRevB.50.17953>.
- ¹⁵ G. Kresse and D. Joubert, *Phys. Rev. B* **59**, 1758 (1999), URL <http://link.aps.org/doi/10.1103/PhysRevB.59.1758>.
- ¹⁶ M. Shishkin, M. Marsman, and G. Kresse, *Phys. Rev. Lett.* **99**, 246403 (2007), URL <http://link.aps.org/doi/10.1103/PhysRevLett.99.246403>.
- ¹⁷ T. M. Schmidt, T. F. E. N. Lima, A. L. da Rosa, R. B. Pontes, and M. C. da Silva, *arXiv:2004.04554v1* (2020).
- ¹⁸ C.-C. Ren, S.-F. Zhang, W.-X. Ji, C.-W. Zhang, P. Li, and P.-J. Wang, *Nanomaterials* **8**, 145 (2018).
- ¹⁹ J. Zhao and H. Zeng, *Phys. Chem. Chem. Phys.* **18**, 9809 (2016).
- ²⁰ C. Si, J. Liu, Y. Xu, J. Wu, B.-L. Gu, and W. Duan, *Phys. Rev. B* p. 115429 (2014).

- ²¹ A. L. da Rosa, E. N. Lima, M. C. da Silva, R. B. Pontes, J. S. de Almeida, T. M. Schmidt, and T. F. m, *J. Phys. Chem. C* **124**, 1170811715 (2020).
- ²² L. Kou, H. Fu, Y. Ma, B. Yan, T. Liao, A. Du, and C. Chen, *Phys. Rev. B* (2018).
- ²³ R. Vivas-Reyes and A. Aria, *Eclat. Quim.* **33**, 69 (2008).
- ²⁴ S. Jiang, S. Butler, E. Bianco, O. D. Restrepo, W. Windl, and J. E. Goldberger, *Nature Communications* **5**, 3389 (2014).
- ²⁵ N. Research, *Nano Research* pp. 546–555 (2017).
- ²⁶ A. N. Rudenko, S. Yuan, and M. I. Katsnelson, *Phys. Rev. B* **92**, 085419 (2015).
- ²⁷ D. Kecik, V. O. Özçelik, E. Durgun, and S. Ciraci, *Phys. Chem. Chem. Phys.* **21**, 7907 (2019), URL [10.1039/C8CP07344A](https://doi.org/10.1039/C8CP07344A).
- ²⁸ X. Chen, C. Tan, Q. Yang, R. Meng, Q. Liang, M. Cai, S. Zhang, and J. Jiang, *J. Phys. Chem. C* **120**, 13987 (2016).
- ²⁹ F. F. Yun, D. L. Cortie, and X. L. Wang, *Phys. Chem. Chem. Phys.* **19**, 25574 (2017).
- ³⁰ Y. Xu, B. Yan, H.-J. Zhang, J. Wang, G. Xu, P. Tang, W. Duan, and S.-C. Zhang, *Phys. Rev. Lett.* **111**, 136804 (2013).